Int. J. Electrochem. Sci., 15 **(2020)** 12264 – 12280, doi: 10.20964/2020.12.35

International Journal of
ELECTROCHEMICAL
SCIENCE
www.electrochemsci.org

Study on the Hydration Processes of High Belite Sulphoaluminate Cement using Electrochemical Impedance Spectroscopy

Shiwei Niu[1], *Funan Sun*[1], *Ruizhen Xie*[2], *Bin He*[1,*], *Fuli Ma*[1], *Xingan Guo*[1], *Atiq Abdul Fattah*[1], *Xingyi Wang*[1], *Pengju Han*[1,*]

[1] College of Civil Engineering, Taiyuan University of Technology, Taiyuan, 030024, China
[2] Mechanics Institute, Jinzhong University, Jinzhong, 030619, China
[*]E-mail: hebin@tyut.edu.cn, 13834569544@163.com

Received: 2 August 2020 / *Accepted:* 28 September 2020 / *Published:* 31 October 2020

This paper aimed to use electrochemical impedance spectroscopy (EIS) to investigate the hydration process of a new generation of cement, as this method has the characteristics of providing energy savings and being environment friendly, and use X-ray diffraction (XRD) to analyse the composition of hydration products at different hydration times. The experimental results suggested that the Nyquist plots of different hydration times had their own distinctive features. In addition, the used equivalent circuit model could provide a good explanation for the experimental phenomenon. The impedance parameters R_{CCP} and R_{CP} increased with increasing hydration time, but the parameter C_{DP} decreased. Correspondingly, the effect of the water-cement ratio on these parameters was completely opposite of that of the hydration time. Furthermore, the results of XRD analysis showed that AFt was the main hydration product in the early stage, and the hydration of C_2S was the main process in the late stage.

Keywords: hydration process; X-ray diffraction; microstructure; electrochemical impedance spectroscopy

1. INTRODUCTION

With the continuous development of human economic society, there is growing demand for engineering materials in the world today. The production volumes of cement, the most important engineering material, keeps pace with the increasing demand. However, the manufacture of Portland cement not only consumes a vast amount of resources and energy but also generates undesirable greenhouse gas emissions [1-2]. China, as the world's largest producer and consumer of cement, is facing enormous challenges of energy conservation and environmental protection. Therefore, the development of a new generation of cement for energy savings and emission reduction plays a pivotal role in the

sustainable development of the cement industry in China [3].

As is fairly well known, the high calcium mineral composition design of Portland cement is the root cause of its high energy consumption and carbon emissions [4]. As early as the 1970s, Mehta proposed that the key to the development of a new generation of cement is to adopt low energy consumption and low carbon emission components instead of high energy consumption and high carbon emission components on the basis of equivalent performances [5]. One such cement called high belite cement (HBC) has been development and reported by many researchers. The mineral composition of this special cement is dominated by dicalcium silicate (C_2S), whose mass fraction is generally greater than 40%. Compared with that of Portland cement, the calcination temperature of HBC is 100-150℃ lower, and energy consumption and greenhouse gas emissions of HBC are significantly lower [6-7]. However, the early strength of this cement is weakened due to the slow hydration rate of C_2S, which limits HBC applications [8].

Calcium sulphoaluminate ($C_4A_3\overline{S}$) has the characteristic of improving the early strength of cement. Moreover, it also has a low CaO content and low calcination temperature, which are similar to the energy saving and emissions reducing characteristics of C_2S [9-10]. Therefore, to address the aforementioned problems of HBC, $C_4A_3\overline{S}$ was used to completely replace tricalcium silicate (C_3S) to form a new generation of cement, namely, high belite sulphoaluminate cement (HBSC). This special cement contains $C_4A_3\overline{S}$ and C_2S as the main mineral components and contains a certain amount of tetracalcium aluminate (C_4AF) and calcium sulphate ($CaSO_4$) [11-13] that is significantly different from that of Portland cement. Generally, HBSC has many excellent properties, such as fast setting, high early strength, good freeze-thaw resistance, excellent impermeability and good corrosion resistance, so it has shown great application potential.

Hydration, a complicated physical-chemical process, is essential for cement materials because it largely determines the microstructure of these materials and then affects their macroscopic performance [14-17]. Much research has been performed on the hydration of Portland cement by various testing methods, which has led to fruitful results [18-19]. However, research on the hydration of HBSC is generally still extremely scarce. It is impossible to establish a direct link between the microscopic mechanism and the macroscopic performance, and thus, the macroscopic performance of HBSC cannot be reasonably explained [20-21].

The purpose of this research is to investigate the hydration process of HBSC through a variety of methods to provide a fundamental basis for the study of its hydration mechanism. X-ray diffraction (XRD) was first used to analyse the composition of hydration products at different hydration times. Then, the changes in the microstructure during the hydration process were investigated by electrochemical impedance spectroscopy (EIS) using a classical equivalent circuit model, and the influence of the water-cement ratio on the cement hydration process was also analysed by impedance parameters.

2. MATERIALS AND EXPERIMENTS

2.1 Experimental materials

For all specimens, HBSC with a strength grade of 42.5 that was obtained from the Polar Bear

Material Company in Tangshan, China was used. The chemical composition and mineralogical composition of the HBSC are presented in Table 1 and Table 2 respectively. Normal tap water was used in the experiment, and there were no other admixtures.

Table 1. Chemical composition of HBSC

Chemical composition	CaO	SiO_2	Al_2O_3	Fe_2O_3	MgO	SO_3	K_2O	Sum	Loss
Mass (%)	50.74	13.98	18.59	2.02	2.15	11.75	0.21	99.44	0.48

Table 2. Mineralogical composition of HBSC

Mineralogical composition	$C_4A_3\bar{S}$	C_2S	f-$CaSO_4$	C_4AF	f-CaO
Mass (%)	34.51	40.08	12.27	6.15	2.06

2.2 Test procedure

In this paper, the specimens were prepared with water-cement ratios of 0.6, 0.8 and 1.0. After mixing thoroughly, the cement pastes were cast into moulds with dimensions of 70.7 mm×70.7 mm×70.7 mm and then stored in a curing chamber (95±5% RH, 20±2℃). Finally, they were extracted from the moulds and returned to the curing chamber until the specified time.

The specimens with a water-cement ratio of 0.6 were crushed at the specified time (1 d, 3 d, 14 d and 28 d). Fragments of approximately 10 mm in size were then soaked in alcohol for 3 d to terminate hydration. Finally, the fragments were removed and ground finely enough to pass through a 0.056 mm sieve. XRD was performed using a LabX XRD-6000 diffractometer made by Shimadzu, Japan. The value of 2θ was pre-set as 5°-50°, and the step size was 0.02°. MDI Jade software was used for XRD analysis.

A CS350 electrochemical workstation was used to measure the electrochemical impedance spectra of cement materials at different hydration times (1 d, 3 d, 7 d, 14 d and 28 d). Copper electrodes with the same size as the cross-sectional area of the specimen were placed at both ends of the specimen. Then, the specimen was fixed to the electrodes with an insulating fixture, and a certain pressure was applied to make the specimen closely contact the electrodes. The schematic diagram of the device is shown in Figure 1.

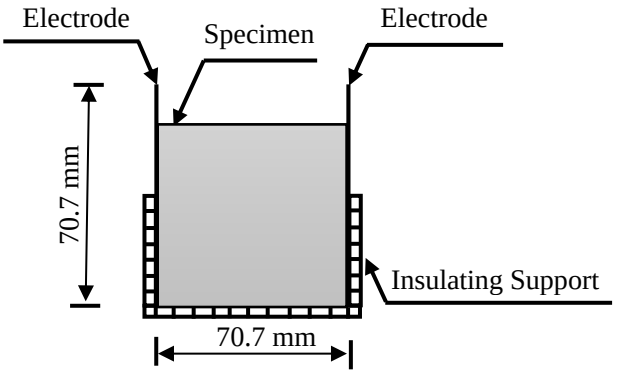

Figure 1. Illustration of the apparatus used for impedance measurements

3. RESULTS AND ANALYSIS

3.1 XRD analysis of hydration products

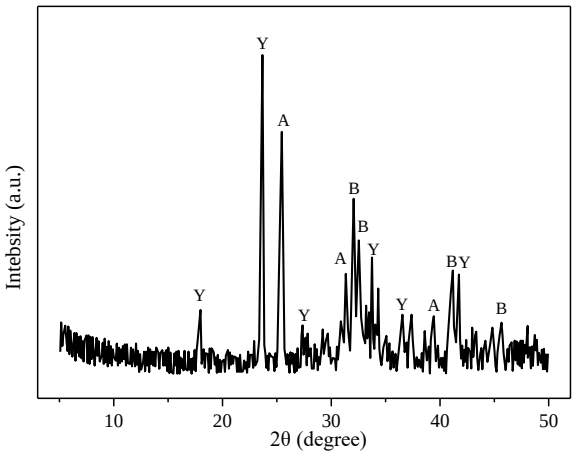

(a) Unhydrated cement

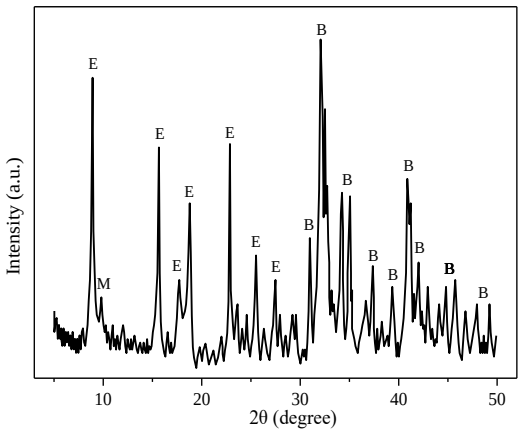

(b) 1 d

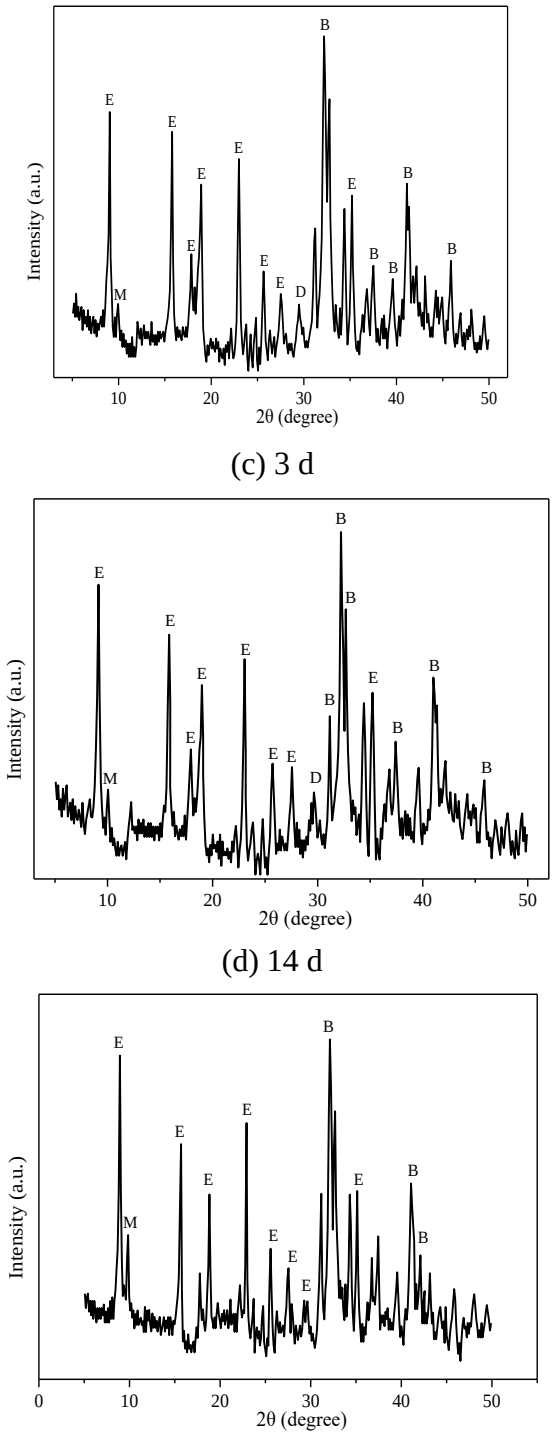

Figure 2. XRD patterns of cement at different hydration times

XRD is one of the most effective methods for the phase identification of cement hydration products [22-23]. Studies have shown that the reactions that may occur during the hydration process of HBSC are as follows [24-25]:

$$C_4A_3\bar{S}+2C\bar{S}+38H \rightarrow C_3A\cdot 3C\bar{S}\cdot 32H+2AH_3 \quad (1)$$

$$C_2S+2H_2O \rightarrow C\text{-}S\text{-}H+CH \quad (2)$$

$$AH_3+3CH+3C\overline{S}+26H_2O \rightarrow C_3A\cdot 3C\overline{S}\cdot 32H \quad (3)$$

$$C_3A\cdot 3C\overline{S}\cdot 32H \rightarrow C_3A\cdot C\overline{S}\cdot 12H+2CSH_2+16H \quad (4)$$

Therefore, according to these reactions, the hydration products of HBSC may include AFt, AH_3, C-S-H, CH and AFm. The XRD results of cement at different hydration times are shown in Figure 2. The significance of the letters in the graphs is as follows: Y, A, B, D, E and M represent $C_4A_3\overline{S}$, $CaSO_4$, C_2S, C-S-H, Aft and AFm, respectively.

Compared with those of unhydrated cement, the characteristic peaks of C_2S are the strongest peaks at 1 d of hydration, which indicates that the hydration level of C_2S is very low. A potential reason for this phenomenon is that the hydration rate of C_2S is low, that is, the reaction of Equation (2) basically does not proceed [26]. The characteristic peaks of AFt can be clearly observed in the XRD pattern, while the characteristic peaks of $C_4A_3\overline{S}$ and $CaSO_4$ disappear. It can be inferred that the reaction shown in Equation (1) occurs during the 1 d hydration process, so $C_4A_3\overline{S}$ and $CaSO_4$ are basically consumed. Furthermore, the characteristic peak of hydration product AFm can also be observed, but the characteristic peak is relatively weak. This is because only a small amount of AFt is transformed into AFm according to Equation (4) at this stage [27-28].

The characteristic XRD peak attributed to C_2S is slightly lower for the sample treated with 3 d of hydration than for the sample treated with 1 d of hydration, and the characteristic peak of C-S-H begins to appear after 3 d of hydration. This shows that the hydration of C_2S is in progress [26], and the amount of unhydrated C_2S is gradually decreasing. Meanwhile, $C_4A_3\overline{S}$ and $CaSO_4$ are completely consumed, and the characteristic peak of AFt becomes more intense [28]. In addition, the characteristic peak of CH is still not observed. There are two causes that may lead to this phenomenon. (1) CH is not generated during the process of cement hydration. (2) CH is generated in the hydration process, but then, it participates in the hydration reaction and is basically consumed as described in Equation (3). Both previous studies and the analysis of this experiment suggest that the latter is the real cause of this phenomenon [25].

From the XRD patterns of the samples after 14 d and 28 d of hydration, it can be observed that the characteristic peaks of C_2S are still very significant, but some of the characteristic peaks disappear with further hydration. The characteristic peaks of AFt are somewhat weakened but remain significant with hydration. In contrast, the characteristic peaks of AFm are quite weak, and even the characteristic peaks are barely visible. In addition, a certain amount of C-S-H began to generate at this stage, but its characteristic peaks are not obvious, which may be attributed to the encapsulation effect existing between the gels [29].

According to the overall analysis of the XRD patterns, AFt is the main hydration product in this new generation of cement, and it is generated in a large amount in the early hydration stage. This is consistent with the research results of the hydration process of sulphoaluminate cement [30], where the only difference is the amount of hydration products. Correspondingly, the late hydration process of this cement is mainly the hydration of C_2S. This result agrees with previous studies on the hydration process of Portland cement [26, 31-32]. In addition, no CH is detected during the entire hydration process.

3.2 Equivalent circuit model

In the process of cement hydration, the change in the microstructure is of considerable importance because it governs the macro-performance of cement materials and has significant influences on their engineering application [33-34]. There are various methods used to investigate the microstructure of cement materials, among which EIS is the most prevalent [35-36]. EIS, a continuous steady-state method, has been demonstrated to be a reliable and efficient technique due to its capability of revealing changes in the microstructure of cement. Furthermore, EIS has advantages in monitoring the microstructure changes of cement under different conditions and in various service environments [37].

The cement specimen is composed of a solid part (hydration products and unhydrated cement) and pores, and its microstructure is schematically illustrated in Figure 3. There are three different conductive paths in such a structure [38]: (1) a continuous conductive path (CCP or Path 1); (2) a discontinuous conductive path (DCP or Path 2); and (3) an "insulator" conductive path (ICP or Path 3). Correspondingly, the microstructure of cement can be simplified as shown in Figure 4, in which the grey area represents the solid part, and the white area represents the pores. In addition, in Figure 4, PS is short for pore solution, and DP is the abbreviation of discontinuous point.

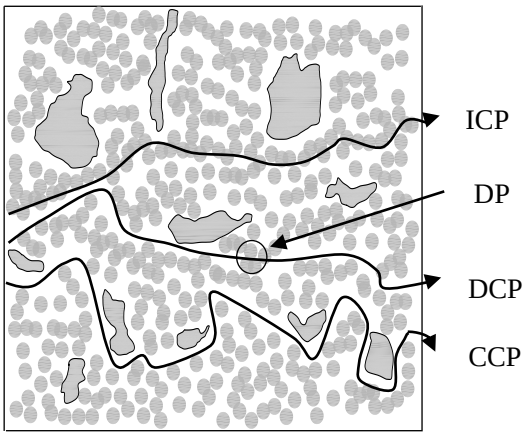

Figure 3. Schematic representation of the microstructure of cement

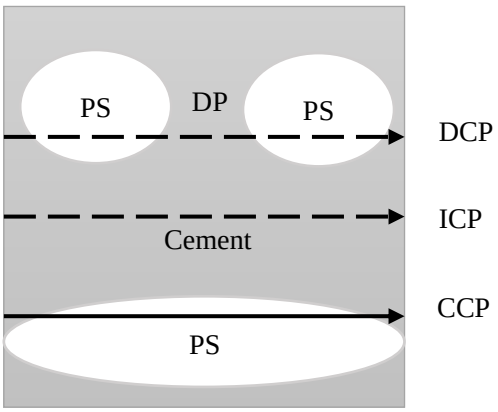

Figure 4. Simplified microstructure of cement

According to previous research [38-40], as shown in Figure 5 (a), an equivalent circuit of cement is proposed. In this model, the equivalent element represents the corresponding conductive path and has a clear physical meaning for the cement microstructure. C_{mat} is the electrical double layer capacitance of the cement matrix; R_{CP} is the resistance of the continuous portion of the DCP; C_{DP} is the electrical double layer capacitance of the discontinuous point of the DCP; R_{CCP} is the resistance of the CCP. In most cases, due to the limitation of electrochemical equipment, C_{mat} is too small to be considered ($C_{mat}\rightarrow 0$). Therefore, the equivalent circuit of cement can be simplified as shown in Figure 5 (b). Compared with the equivalent circuit proposed by Han et al. [41], such an equivalent circuit is simple.

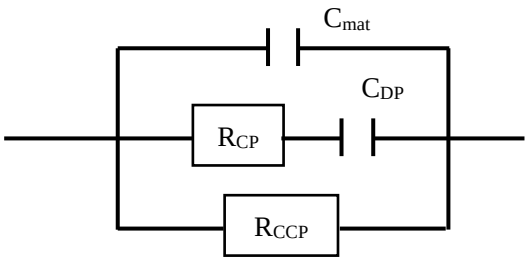

(a) Detailed equivalent circuit

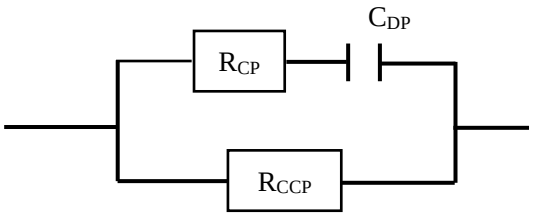

(b) Simplified equivalent circuit

Figure 5. Equivalent circuit for the microstructure of cement

In the experiment, the current is first transmitted through the electrode to the surface of the specimen and then conducted inside the specimen. Therefore, the electrode effect cannot be ignored. As a result, a typical equivalent circuit model considering the electrode effect is proposed [42], which is described as R_s (C_1R_{ct1}) (C_2R_{ct2}) (Figure 6). The circuit of the cement matrix is located within the dashed box, which differs from the circuit of the electrode effect in the model, so the two parts can be well separated.

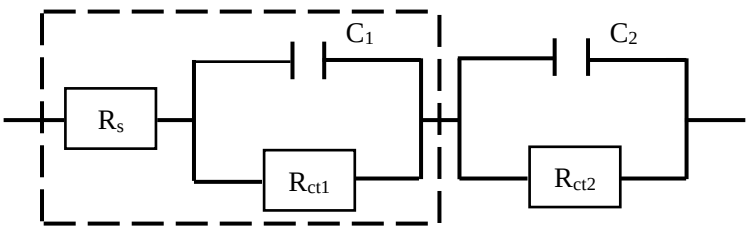

Figure 6. The typical circuit of cement

Based on the equivalent model and theoretical calculation of cement matrix, there are two more critical parameters, R_s and R_{ct1} [43]. R_s, the intersection point of the high frequency region and the horizontal axis, is the electrolyte resistance in the pore solution [44-45]. R_{ct1}, the diameter of the high-frequency semicircle, is closely related to the microstructure of cement materials [45].

By comparing the typical equivalent circuit model (Figure 6) with the equivalent circuit (Figure 5(b)) and based on relevant research, the following relationships can be established [38, 46-47]. These transformations make it easy to extract the capacitance and resistance that characterize the microstructure changes of cement materials. Furthermore, these transformation make the measured impedance parameters, such as R_s, R_{ct1}, and C_1, more meaningful [38].

$$R_{CCP} = R_s + R_{ct1} \tag{5}$$

$$R_{CP} = \left(R_s + R_{ct1}\right) R_s / R_{ct1} \tag{6}$$

$$C_{DP} = C_1 \left[R_{ct1} / \left(R_s + R_{ct1}\right) \right]^2 \tag{7}$$

Equation (5) shows that the value of R_{CCP} increases with decreasing numbers of continuous pores in the cement material. That is, the increase in the sum of R_s and R_{ct1} indicates that the continuous pores are gradually blocked by hydration products in the hydration process [38, 47]. According to Equation (6), the resistance of the continuous portion of DCP, R_{CP}, is determined by two parts, (R_s+R_{ct1}) and (R_s/R_{ct1}). This is because some of the CCP paths turn into DCP paths after the continuous pores are blocked by hydration products, thus affecting the value of R_{CP} [47]. Moreover, C_{DP} is related to the thickness of the discontinuous points, and its value can well reflect the development of the compactness of cement materials during hydration processes [38]. From Equation (7), R_{ct1} is the major factor used to determine the value of C_{DP}, since it is far greater than the value of R_s.

3.3 EIS analysis of the hydration process

3.3.1 Analysis of Nyquist plots

A Nyquist plot is often used in the analysis of electrochemical impedance spectroscopy (EIS) results and considers both the real part (Z') and imaginary part (Z'') of the impedance. The hydration of cement is a process by which cement particles turn into hydration products, such as Aft and C-S-H gel. In general, hydration products have much larger volumes than cement particles. Therefore, the increase in the volume of the solid phase is more likely to block continuous pores and to narrow discontinuous pores or thicken the discontinuous point layers [38]. All these changes will cause the Nyquist plots to change with respect to hydration time, so the Nyquist plots have different characteristics at different hydration times. The Nyquist plots of the cement specimens with water-cement ratios of 0.6, 0.8 and 1.0 are shown in Figure 7.

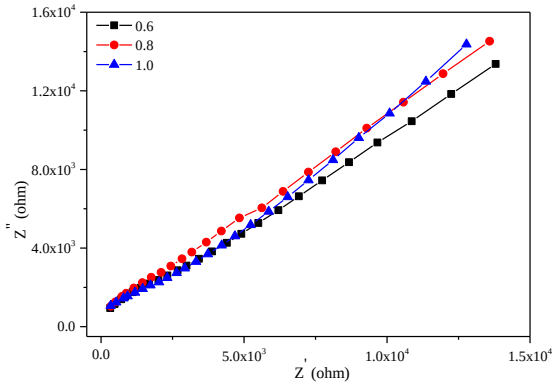

(a) 1 d

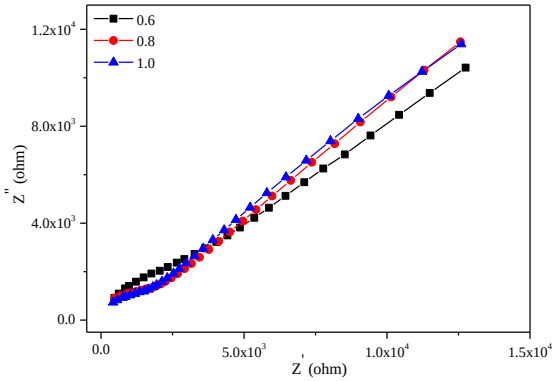

(b) 3 d

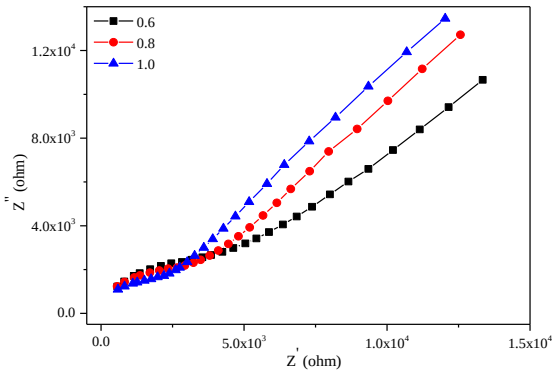

(c) 7 d

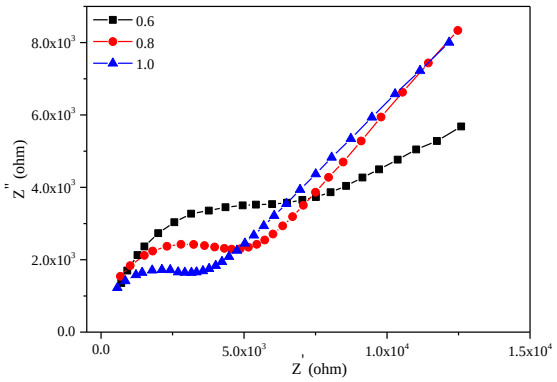

(d) 14 d

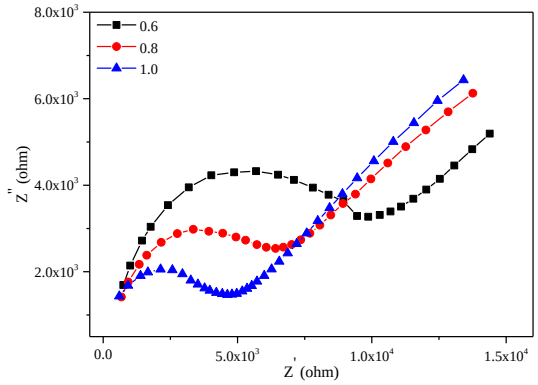

(e) 28 d

Figure 7. Nyquist plots of cement specimens at different hydration times

As shown in Figure 7 (a), the Nyquist plot of cement hydrated for 1 d is basically a straight line without a capacitive loop in the high-frequency region. This is because the hydration degree of cement particles in the initial stage is still very low, and the filling effect of hydration products is not significant [48]. Most of the intervals between the solid phases are not blocked but are filled with water. As a result, the cement specimens are full of CCP paths, with few or no DCP paths. The simplified equivalent circuit (Figure 5 (b)) can be further simplified to only one element (R_{CCP}), which cannot show a capacitive loop in the Nyquist plot [38, 47].

After hydration for 3 to 7 d, as shown in Figure 7(b, c), the impedance curve possesses a slight protuberance in the high-frequency region, and a capacitive loop tends to appear. Relevant research shows that the appearance of a capacitive loop in the high-frequency region is directly related to the resistance of the solid phase of the specimen [38, 49]. This indicates that a certain amount of C-S-H gel has accumulated in the specimen at this stage, which is in agreement with the results of XRD analysis.

It is evident from Figure 7 (d) that after 14 d of hydration, a relatively complete capacitive loop appears in the high-frequency region. This proves that a considerable amount of C-S-H gel has accumulated in the specimen. After 28 d of hydration, as shown in Figure 7 (e), the capacitive loop is more complete than that observed the previous stage. Thereafter, cement hydration is in a stable stage, and the shape of the Nyquist plot is no longer significantly different; instead, there is a slight movement in its position [47, 50].

3.3.2 Analysis of impedance parameters with hydration time

The values of impedance parameters for different hydration times based on the typical equivalent circuit (Figure 6) are shown in Table 3. Then, according to Equation (5), (6) and (7), the corresponding impedance parameters are shown in Figure 8, 9 and 10.

The values of the impedance parameter R_{CP} of the cement materials at different hydration times are shown in Figure 8. At the beginning of the tests, the R_{CP} values increase sharply, and then, the increase in the R_{CP} value slows markedly. For example, in the process of hydrating from 1 d to 7 d, the R_{CP} value increases by 164 ohm for the specimen with a water-cement ratio of 1.0, while its R_{CP} value

increases by only 12 ohm in the process of hydrating from 7 d to 28 d. The reasons for this different behaviour are as follows: the hydration products quickly fill the pores in the early stage of hydration, resulting in a rapid decrease in porosity, and then, there is less space for the hydration products to fill, that is, the porosity decreases slowly. Overall, the R_{CP} value increases at the same rate that the number of hydration days increases. This is consistent with the change trend of the porosity of Portland cement in the literature [47, 51].

Table 3. The values of impedance parameters with different water cement ratios

Hydration time (d)	R_s(ohm)			R_{ct1}(ohm)			C_1(pF)		
	Water-cement ratio			Water-cement ratio			Water-cement ratio		
	0.6	0.8	1.0	0.6	0.8	1.0	0.6	0.8	1.0
1	51	44	32	1919	1472	1202	1010	1250	1310
3	144	108	75	2202	1537	1400	939	1170	1170
7	203	145	98	3165	2281	1497	888	923	1010
14	249	173	109	5842	4096	2630	814	873	986
28	281	185	113	8158	5362	3938	759	767	813

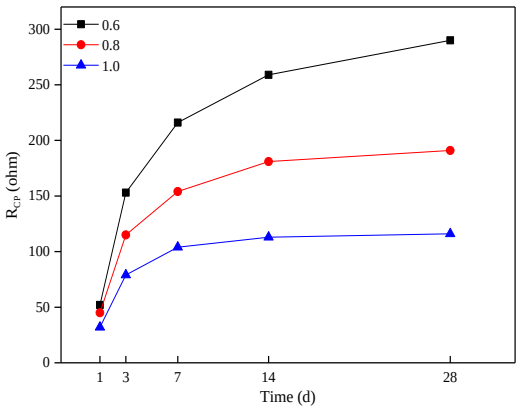

Figure 8. The values of impedance parameter R_{CP} for different hydration times

The values of the impedance parameter R_{CCP} of the cement materials at different hydration times are shown in Figure 9. Similar to R_{CP}, R_{CCP} also shows an increasing trend with the increase of hydration time. However, the effects of hydration time on the growth of R_{CCP} and R_{CP} are different. Comparatively, the overall impact of hydration time on the value of R_{CCP} is much more significant than that on R_{CP}. For example, for the specimen with a water-cement ratio of 0.6, the R_{CCP} value at 28 d increases by 6469 ohm compared with its initial value, while the R_{CP} value only increases by 238 ohm compared with its initial value. There are at least two reasons for such a result [38, 52]. (1) Hydration products can block the CCP paths so that the number of CCPs decreases, whereas hydration products can only narrow the DCPs or increase the thickness of the layer of a discontinuous point. (2) The transformation of some CCPs into DCPs will counteract the increase in R_{CP} value to some extent. Furthermore, the ratio of R_{CCP}/R_{CP} increases as the hydration time increases. This is because the CCPs, which play a major role in electric conduction, cannot be completely turned into DCPs after being blocked [47].

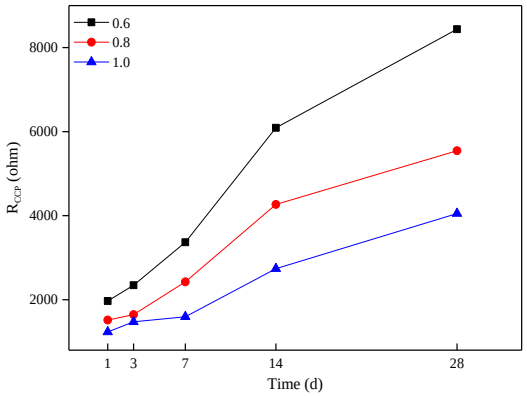

Figure 9. The values of impedance parameter R_{CCP} for different hydration times

The values of the impedance parameter C_{DP} of the cement materials at different hydration times are shown in Figure 10. Compared with R_{CP} and R_{CCP}, the changes in the C_{DP} values exhibit the opposite trend. The values of C_{DP} decrease sharply at the beginning of the test, and then, the decreasing trend slows. According to the previously proposed equivalent circuit model [38, 47], the reason for the decrease in the C_{DP} value is that the hydration products will increase the thickness of the discontinuous point in DCPs. Therefore, this different behaviour indicates that hydration products are generated rapidly in the early stage of hydration, and then, the hydration reaction rate decreases [11]. This is consistent with the results of XRD.

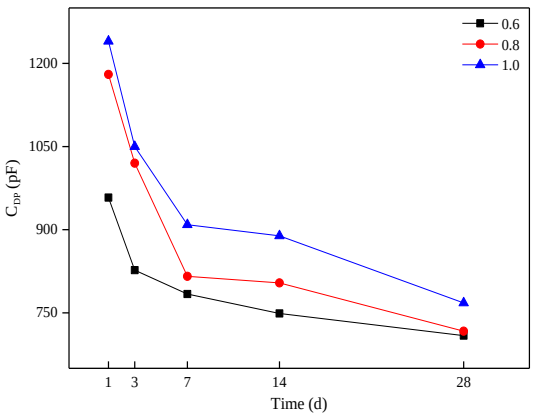

Figure 10. The values of impedance parameter C_{DP} for different hydration times

3.3.3 Analysis of impedance parameters with water-cement ratio

The water-cement ratio has significantly influenced the cement hydration process and the development of the cement microstructure [38, 53]. Changes in the water-cement ratio typically alter the porosity of cement materials, and thus, the impedance parameters change with changing the water-cement ratio. By combining the results of previous research, the value of R_{CCP} is considered to be an effective indicator of the degree of cement hydration [47]. As seen from the Figure 11, after 1 d of hydration, the R_{CCP} values of the specimens with water-cement ratios of 0.6, 0.8 and 1.0 are 1970, 1516, and 1234 ohm, respectively. This shows that the degrees of cement hydration at this stage are not very different. Afterward, as hydration proceeded, a lower water-cement ratio will lead to a greater value of

R_{CCP}. After 7 d of hydration, the R_{CCP} value of the specimen with a water-cement ratio of 0.6 is more than twice that of the specimen with a water-cement ratio of 1.0. This shows that the hydration degree of the latter is lower than that of the former [38, 47]. With further development of hydration processes, the increase in the compactness and pore structure complexity of cement materials will be reflected by an increase in impedance parameter R_{CCP} [54]. It is not difficult to observe from Figure 11 that the R_{CCP} values of the specimen with a water-cement ratio of 0.6 at 14 d and 28 d are far greater than those of the other two groups, and the difference further increases. This demonstrates that the hydration degree of the specimen with a low water-cement ratio is much greater than that with a high water-cement ratio.

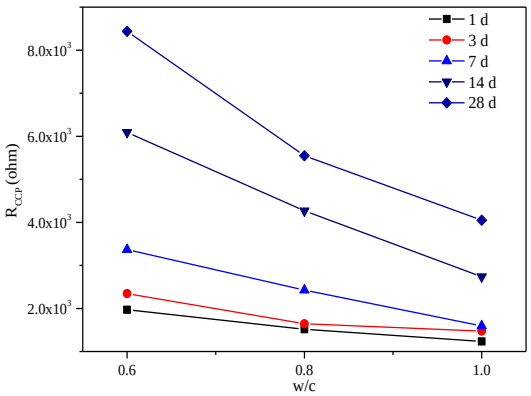

Figure 11. R_{CCP} values of specimens with different water-cement ratios

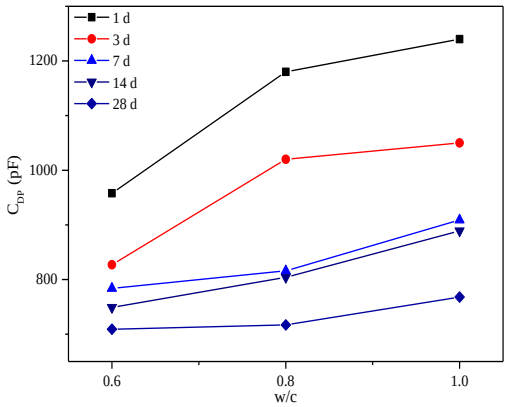

Figure 12. C_{DP} values of specimens with different water-cement ratios

Additionally, the C_{DP} values of the specimens with different water-cement ratios are shown in Figure 12. As can be observed, the water-cement ratio has a significant effect on the value of C_{DP}, especially at the initial period of hydration. For example, the C_{DP} value of the specimen with a water-cement ratio of 0.6 at 1 d of hydration is 282 pF greater than that of the specimen with a water-cement ratio of 1.0. This reveals that the water-cement ratio plays a prominent role in increasing the thickness of the layer of the discontinuous point [38, 55]. However, at 28 d of hydration, there is no difference between the C_{DP} values of the specimens with different water-cement ratios. For example, the C_{DP} value of the specimen with a water-cement ratio of 0.6 is only 59 pF greater than that of the specimen with a

water-cement ratio of 1.0. This shows that the effect of the water-cement ratio is significantly weakened with the hydration process [55].

4. CONCLUSIONS

In this paper, the hydration process of HBSC was investigated by XRD and EIS. XRD analysis was employed to analyse the composition of hydration products at different hydration times, and EIS was performed to study the microstructure changes of cement materials during the whole hydration process. The main conclusions drawn from this study were as follows:

1) The hydration product of this new generation of cement in the early stage was mainly AFt; the concentration of calcium sulphate would decrease with the hydration process, so the transformation of partial AFt into AFm was observed; the late stage of hydration mainly included the hydration of C_2S, and a certain amount of C-S-H was generated; no CH was detected during the entire hydration process.

2) The Nyquist plots of this new generation of cement had their own distinctive features at different hydration times. Since the specimens were full of CCPs and had few or no DCPs in the early stage of hydration, the Nyquist plot in the high-frequency region was basically a straight line. Afterward, as hydration proceeded, the high-frequency region gradually transitioned into a complete capacitive loop. This undoubtedly demonstrated that a considerable amount of C-S-H gel was generated.

3) An equivalent circuit model containing impedance parameters R_{CP}, C_{DP} and R_{CCP} was employed for cement materials. These parameters could be easily calculated from the measured parameters R_s, C_1 and R_{ct1} and had been demonstrated to have clear meanings. Therefore, this model successfully explained the experimental phenomena observed from the data.

4) Impedance parameters R_{CCP} and R_{CP} increased with increasing hydration time throughout the entire hydration process. This indicated that the compactness and pore structure complexity of cement materials increased throughout the hydration process. In contrast, the opposite trend was observed for impedance parameter C_{DP}. This was mainly due to the increase in the thickness of the layer of the discontinuous point. Furthermore, the effect of the water-cement ratio on these parameters could not be neglected.

ACKNOWLEDGEMENTS
The author would like to express his sincere gratitude to Professor Han Pengju for his guidance, support and encouragement. The author should also thank the financial support provided by the National Natural Science Foundation of China (No. 41807256/51208333), the Special Talent Project of Shanxi Province (Science and Technology Innovation Project for Outstanding Talents 2019), the PhD Research Launch Project of Jinzhong University, Scientific and Technological Innovation Projects of Colleges and Universities in Shannxi Province and Opening Project of Sichuan University of Science and Engineering, Material Corrosion and Protection Key Laboratory of Sichuan Province (No. 2020CL13).

References

1. E. Crossin, *J. Clean. Prod.*, 95 (2015) 101.
2. F. Winnefeld and B. Lothenbach, *Cem. Concr. Res.*, 40(8) (2010) 1239.

3. J.S. Damtoft. *Cem. Concr. Res.*, 38(2) (2008) 115.
4. M. Schneider, M. Romer and M. Tschudin, *Cem. Concr. Res.*, 41(7) (2011) 642.
5. E. Gartner, *Cem. Concr. Res.*, 34(9) (2004) 1489.
6. T.B. Sui, K. Z. Liu, J. Wang, S.H. Guo, Y. Liu and P. Zhao, *J. Chin. Ceramic Soc.*, 27(4) (1999) 106.
7. S.H. Guo, Z. Lin, J.H. Su, H.T. Zhang and Y.M. Chen, *J. Chin. Ceramic Soc.*, 28(S1) (2000) 16.
8. T. Stanek and P. Sulovsky, *Cem. Concr. Res.*, 68 (2015) 203.
9. J. Pera and J. Ambroise, *Cem. Concr. Res.*, 34(4) (2004) 671.
10. L. Pelletier, F. Winnefeld and B. Lothenbach, *Cem. Concr. Comp.*, 33(5) (2011) 551.
11. I. Janotka, L. Krajci, A. Ray and S.C. Mojumdar, *Cem. Concr. Res.*, 33 (2003) 489.
12. A. Rungehet, P. Chindaprasirt, S. Wansom and K. Pimraksa, *J. Clean. Prod.*, 115(12) (2015) 273.
13. E. Costa and B.D. Eugênio, *Constr. Build. Mater*., 122(9) (2016) 373.
14. X.Y. Pang, D.P. Bentz, C. Meyer, G.P. Funkhouser and R. Darbe, *Cem. Concr. Comp.*, 39(5) (2013) 23.
15. J.R. Zhang, T.Y. Fan, H.Y. Ma and Z.J. Li, *Constr. Build. Mater*., 88 (2015) 118.
16. S.W. Tang, X.H. Cai, Z. He, W. Zhou, H.Y. Shao, Z.J. Li, T. Wu and E. Chen, *Constr. Build. Mater*., 146 (2017) 15.
17. A. Guerrero, A. María, M. Gutiérrez and Ruby, *Constr. Build. Mater*., 193 (2018) 518.
18. A. Rungchet, C.S. Poon, P. Chindaprasirt and K. Pimraksa, *Cem. Concr. Comp*., 83 (2017) 10.
19. A. Guerrero, A. María, M. Gutiérrez and Ruby, *Constr. Build. Mater*., 193 (2018) 518.
20. T. Pajkossy and R. Jurczakowski, *Curr. Opin. Electrochem*., 1(1) (2017) 53.
21. B.Q. Dong, G. Li, J.C. Zhang, Y.Q. Liu, F. Xing and S.X. Hong, *Constr. Build. Mater*., 149 (2017) 467.
22. J.W. Bullard, H.M. Jennings, R.A. Livingston, A. Nonat, G.W. Scherer, J.S. Schweitzer, K.L. Scrivener and J.J. Thomas, *Cem. Concr. Res.,* 41(12) (2010) 1208.
23. J. Goergens, T. Manninger and F. Goetz-Neunhoeffer, *Cem. Concr. Res.,* 136 (2020) 106.
24. M.Z Lan, B.F. Xiang, J. Zhou, Z.X. Ge and C.J. Liu, *B. Chin. Ceram. Soc*., 36 (8) (2017) 2720.
25. S.G. Mei and S.M. Song, *J. Wuhan Univ. Technol.*, 31(7) (2009) 1.
26. J.Y. Li and J. Chang, *Constr. Build. Mater*., 208 (2019) 36.
27. H. Zhen, H. Yang and M. Liu, *J. Wuhan Univ. Technol. (Mater. Sci. Ed.)*, 29 (2014) 70.
28. M. García-Maté, I. Santacruz, G. De la Torre, L. León-Reina and A.G. Aranda, *Cem. Concr. Comp*., 34 (2012) 684.
29. W.G. Li, Z.Y. Huang, G.Q. Hu, W.H. Duan and S.P. Shah, *Constr. Build. Mater*., 131 (2017) 767.
30. B. Ma, X.R. Li, X.D. Shen, Y.Y Mao and H. Huang, *Constr. Build. Mater*., 52 (2014) 261.
31. K. Yilmaz, *J. Build. Eng*., 31 (2020) 101419.
32. D. Guillaume, M. Sandrine, G. philippe, G. Etienne, G.M. Marielle, D. Dinarzed, A. Sofiane and F. Fabienne, *Constr. Build. Mater*., 244 (2020) 950.
33. B. Lothenbach, K. Scrivener and R.D. Hooton, *Cem. Concr. Res*., 41(3) (2011) 217.
34. F. Saly, L.P. Guo, R. Ma, C.P. Gu and W. Sun, *J. Wuhan Univ. Technol. (Mater. Sci. Ed.),* 33(6) (2018) 1444.
35. S.W. Tang, X.H. Cai, Z. He, W. Zhou, H.Y. Shao, Z.J. Li, T. Wu and E. Chen, *Constr. Build. Mater*., 146 (2017) 15.
36. T. Pajkossy and R. Jurczakowski, *Curr. Opin. Electrochem*., 1(1) (2017) 53.
37. B.Q. Dong, J.C. Zhang, Y.Q. Liu, G.H. Fang, Z. Ding and F. Xing, *Constr. Build. Mater*., 113 (2016) 997.
38. G.L. Song, *Cem. Concr. Res.*, 30 (2000) 1723.
39. P. Lawrence, M. Cyr and E. Ringot, *Cem. Concr. Res.*, 33 (2003) 1939.
40. P. Gu, P. Xie and J.J. Beaudoin, *Cem. Concr. Rrs.*, 23(1) (1993) 157.
41. P.J. Han, Y.F. Zhang, Y.C. Frank and X.H. Bai, *J. Cent. South Univ.*, 22 (2015) 4318.
42. F.Q. He, R.P. Wang, C.J. Shi, R.X. Zhang, C.P. Chen, L. Lin and X.P. An, *Constr. Build. Mater*.,

143 (2017) 179.
43. D.D. Macdonald, *Electrochim. Acta*，51 (8-9) (2006) 1376.
44. H. Ma and Z. Li, *Comput. Concr*., 11(4) (2013) 317.
45. C. Cetin, S.T. Erdogan and M. Tokyay, *Cem. Concr. Comp*., 67 (2015) 39.
46. X. Wang and H. Lee, *Cem. Concr. Res.*, 40 (2010) 984.
47. X.P. An, C.J. Shi, F.Q. He and D.H. Wang, *J. Chin. Ceramic Soc.*, 40(7) (2012) 1059.
48. M. Cabeza, P. Merino and A. Miranda, *Cem. Concr. Res*., 32 (2002) 881.
49. D.E. Macphee, D.C. Sinclair and S.L. Stubbs, *J. Mater. Sci. Lett.,* 15 (1996) 1566.
50. L. Chi, Z. Wang, S. Lu, D.Z. Zhao and Y. Yao, *Constr. Build. Mater*., 208 (2019) 659.
51. L.C. Zhang and J.K. Zhou, *Constr. Build. Mater*., 259 (2020) 119856.
52. M.L. Shi, *Impedance Spectroscopy of Concrete*, China Railway Press, (2003) Beijing, China.
53. N. Morteza, T. Azim, A. Iman and A. Farhad, *Constr. Build. Mater.,* 237 (2020) 985.
54. W.J. Long, Y.C. Gu, F. Xing and K.H. Khayat, *Cem. Concr. Comp.*, 194 (2018) 72.
55. P. Rovnaník, I. Kusák, P. Bayer, P. Schmid and L. Fiala, *Cem. Concr. Rrs.*, 118 (2019) 84.